JACS
JOURNAL OF THE AMERICAN CHEMICAL SOCIETY

pubs.acs.org/JACS Article

Isomerization and Selective Hydrogenation of Propyne: Screening of Metal−Organic Frameworks Modified by Atomic Layer Deposition

Ryan A. Hackler,[$] Riddhish Pandharkar,[$] Magali S. Ferrandon, In Soo Kim, Nicolaas A. Vermeulen, Leighanne C. Gallington, Karena W. Chapman, Omar K. Farha, Christopher J. Cramer, Joachim Sauer,[*] Laura Gagliardi,[*] Alex B. F. Martinson,[*] and Massimiliano Delferro[*]

Cite This: https://dx.doi.org/10.1021/jacs.0c08641

ABSTRACT: Various metal oxide clusters upward of 8 atoms (Cu, Cd, Co, Fe, Ga, Mn, Mo, Ni, Sn, W, Zn, In, and Al) were incorporated into the pores of the metal−organic framework (MOF) NU-1000 via atomic layer deposition (ALD) and tested via high-throughput screening for catalytic isomerization and selective hydrogenation of propyne. Cu and Co were found to be the most active for propyne hydrogenation to propylene, and synergistic bimetallic combinations of Co and Zn, along with standalone Zn and Cd, were established as the most active for conversion to the isomerized product, propadiene. The combination of Co and Zn in NU-1000 diminished the propensity for full hydrogenation to propane as well as coking compared to its individual components. This study highlights the potential for high-throughput screening to survey monometallic and bimetallic cluster combinations that best affect the efficient transformation of small molecules, while discerning mechanistic differences in isomerization and hydrogenation by different metals.

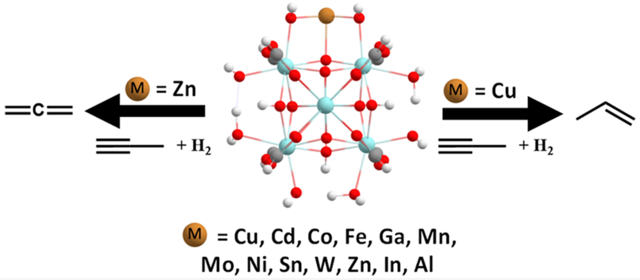

INTRODUCTION

Selective hydrocarbon catalysis is vital for the production of fuels and chemical intermediates needed in various industries.[1,2] Selective alkyne hydrogenation, for example, is necessary in alkene polymerization processes to avoid both poisoning of the catalyst by alkyne impurities and full hydrogenation to low-value alkane products.[3] Generally, the alkyne impurities in the olefin feed competitively bind to the active sites of the catalyst, preventing adsorption and polymerization of the alkene.[4,5] Isomers like the corresponding allene usually require partial hydrogenation in polymerization catalysis as well, as the diene also acts as a potent poison. Selective conversion of alkynes to the diene isomer, however, can produce other important chemical intermediates needed en route to various classes of pharmaceuticals such as steroids.[6,7] In the case of selective alkyne isomerization, base-mediated homogeneous and heterogeneous catalysis has only been shown to exhibit up to 15% selectivity for simple allenes.[8,9] Generally, this is due to simple alkynes being thermodynamically more favorable than their isomers. The isomerization mechanism involves either a carbocation or carboanion intermediate depending on how protons are abstracted via the active site.

Recent investigations into the use of metal−organic frameworks (MOFs) as tunable supports for single-site metal catalysts have shown great promise for the selective transformation of a multitude of hydrocarbons, including light alkanes.[10−12] MOFs are crystalline porous materials comprised of a metal node and organic linker molecules with accessible functional groups within the pores.[13] The well-defined structure and porosity of MOFs mean this unique class of materials is well-equipped to act as a scaffold for catalytically active and uniform metal clusters. Metal nanoparticles and clusters possess unique catalytic properties due to their size,[14] so any synthetic approach that can produce uniform active sites on a viable support proves invaluable for producing selective catalysts and studying the mechanisms behind the active sites. MOFs can behave as selective hydrocarbon transformation catalysts when coupled with a developed and thorough understanding of how to deposit metal clusters.

In this study, NU-1000 was chosen as the MOF to support the various metal oxide species. NU-1000 is a zirconium based MOF with $[Zr_6(\mu_3\text{-}O)_4(\mu_3\text{-}OH)_4(OH)_4(OH_2)_4]^{8+}$ nodes and tetratopic 1,3,6,8-tetrakis(*p*-benzoate)pyrene linkers (Figure 1).[15] Hydroxyl (−OH) and aquo (−OH$_2$) groups reside at the Zr node within 31 Å sized pores and allow for the incorporation of various metals through postsynthetic

Received: August 11, 2020

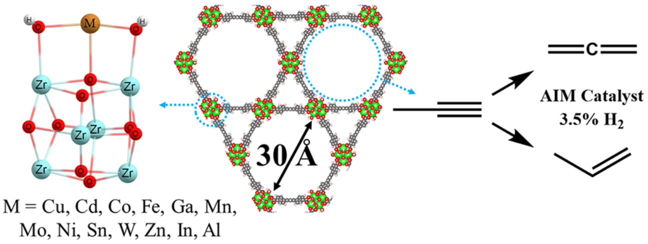

Figure 1. Reaction scheme for selective propyne isomerization and hydrogenation to alkenes via AIM catalysts, with the idealized AIM structure shown to the left. Metal ions (denoted M) attached onto the Zr_6 oxide node include Cu, Cd, Co, Fe, Ga, Mn, Mo, Ni, Sn, W, Zn, In, and Al.

modification.[16] These modifications can be undertaken through atomic layer deposition (ALD): a vapor-phase technique used to synthesize thin films, nanoparticles, and single atom catalysts of various compositions on a myriad of supports.[17] Metalation of MOFs via reaction with volatile metalorganics or ALD in MOFs (AIM) has been leveraged for the construction of hydrocarbon catalysts for hydrogenation of ethylene and *m*-nitrophenol, oxidative dehydrogenation of propane, and dehydration of ethanol.[18−22] The promise of AIM catalysts lies in the potential to synthesize small metal clusters of various compositions with precision in the size and nature of the cluster. Metal clusters can range in size from one to several atoms within a single pore. The size of the pore also allows for enhanced selectivity of the reactant for transformation.[23]

In this work, various metals including Cu,[24,25] Cd,[25] Co,[25] Fe,[25] Ga,[25] Mn,[25] Mo,[25] Ni,[19] Sn,[25] W,[25] Zn,[16,25] In,[25] and Al[21,25] were incorporated into NU-1000 using methods described previously and fully characterized. The postsynthetically modified MOFs were monitored at various temperatures (50−300 °C) for propyne hydrogenation to propylene via high-throughput screening. Simultaneously, the isomerization product was observed under hydrogenation conditions. Bimetallic combinations of Co−Zn and Zn−Co were also explored for any synergistic effects. Thermogravimetric and metal loading analyses were performed to provide insight into the active site environment. Isomerization and hydrogenation pathways for Cu and Zn AIMs were then determined, and their energies were calculated via density functional theory (DFT). This work showcases a comprehensive suite of AIM catalysts and explores their activity and selectivity for propyne transformation.

■ EXPERIMENTAL SECTION

Synthesis of NU-1000. $ZrOCl_2·8H_2O$ (97 mg, 0.30 mmol) and benzoic acid (2.70 g, 22 mmol) were mixed in 8 mL of DMF (in a 6-dram vial) and dissolved using sonication. The clear solution was incubated in an oven at 80 °C for 1h. After being cooled to room temperature, 1,3,6,8-tetrakis(*p*-benzoic acid)pyrene (H_4TBAPy, 40 mg, 0.06 mmol) was added to this solution and the mixture was sonicated for 10 min. The yellow suspension was heated in an oven at 100 °C for 18 h. After being cooled to room temperature, a yellow NU-1000 precipitate was collected by centrifugation (7800 rpm, 5 min) and washed with fresh DMF twice. As synthesizedNU-1000 was then suspended in 13 mL of DMF, and 0.5 mL of 8 M HCl was added to this mixture to acid-activate the zirconium node. This mixture was heated in an oven at 100 °C for 24 h. After being cooled to room temperature, the supernatant was removed by centrifuge, and the material was washed twice with fresh DMF. Subsequently, the solid materials were washed twice with acetone and soaked in acetone for an additional 12 h. Then the acetone was removed by centrifugation, and the solid was briefly dried in an oven at 80 °C. The solid material was activated on a SmartVacPrep station (Micromeritics) under dynamic vacuum at 120 °C until an outgassing rate of ≤0.002 mmHg min^{-1} was reached.

Atomic Layer Deposition in Metal−Organic Frameworks (AIM). Hydration of NU-1000 was conducted using a modified procedure described previously.[26] In each AIM experiment, 10−60 mg of NU-1000 powder was heated to 115 °C under a rough vacuum with a continuous flow of 20 sccm nitrogen (N_2) resulting in 0.4 Torr base pressure−standard "purge" conditions. After 10 min of purge conditions to remove any physisorbed water, the powder was reproducibly hydroxylated and hydrated with a 60 s exposure to water vapor using a pulse sequence of t_1-t_2-t_3 (pulse−exposure−purge), where t_1 = 1 s, t_2 = 59 s, t_3 = 60 s. Subsequently, the powder was purged for 5 min again to remove physisorbed water and obtain a reproducible − OH and − OH_2 population.

After the sample preparation procedure outlined above, exposure to a variety of volatile organometallic precursors afforded the metal-modified MOFs tested for catalysis. A complete list of the ALD procedures used can be found in the SI. In one example, Co-AIM was performed by introducing dicarbonyl(cyclopentadienyl) cobalt(I) (Strem Chemicals, min. 95%) into the reaction chamber using the pulse sequence as for water, but with standard pulse times of t_1 = 0.75 s, t_2 = 59.25 s, and t_3 = 60 s. Following 80 repeated exposures of $CpCo(CO)_2$, which constitute a single ALD half-cycle, the sample was left to purge for an additional 5 min to ensure a complete removal of any excess precursor and/or reaction byproducts within the pores of NU-1000. The powder was subjected to 60 doses of water vapor according to the previous dosing schedule but with shorter pulse length (0.1 s) in order to minimize the effects of MOF heating expected from the strongly exothermic heat of reaction.[27] The metal loading of each resulting AIM is summarized below in Table 1. The production of the A-B AIMs (i.e., Co−Co AIM, Co−Zn AIM, Zn−Co AIM, and Zn−Zn AIM) was achieved by performing a single ALD cycle each of A-AIM followed by B-AIM.

High-Throughput Catalyst Testing. Selective hydrogenation of propyne was performed in a 16 fixed bed reaction system (Flowrence, Avantium). Typically, 5 mg of as-prepared catalyst was diluted with 50 mg nonporous silica gel (Davisil 230−400 mesh) and loaded into a quartz reactor (inner diameter = 2 mm, outer diameter = 3 mm, length = 300 mm). The silica diluent showed no catalytic activity in control experiments. Reactions were performed between 50 and 300 °C at a heating rate of 5 °C/min and pressure ranged from 1 to 10 atm. All gases were purchased from Airgas. 2% propyne in Ar was used with 3.5% H_2 in Ar for selective hydrogenation experiments. N_2 (ultrahigh purity (UHP)) was sometimes added to keep a constant gas hourly space velocity (GHSV) and was also used to sweep gas to the gas chromatograph (GC) after reaction. He (UHP) was used as the standard for GC. Flow rates of 5.3 mL/min of 2% propyne in Ar, 3.1 mL/min of 3.5% H_2 in Ar, and 1 mL/min He were used per reactor giving a propyne/H_2 ratio of 1 and a GHSV of 3015 h^{-1}. Additional experiments were conducted at flow rates of 2.8 mL/min of 2% propyne in Ar, 3.1 mL/min of 3.5% H_2 in Ar, 2.5 mL/min N_2, and 1 mL/min He per reactor giving a propyne/H_2 ratio of 2 and a GHSV of 3015 h^{-1}.

The effluent of each reactor was analyzed sequentially by a gas chromatograph (7890B, Agilent Technologies), equipped with a

Table 1. Metal Atoms Per Zr_6 Node for Each Single-Cycle AIM as Determined by ICP-OES[25]

Metal	Cu	Cd	Co	Fe	Ga	Mn	Mo	Ni	Sn	W	Zn	In	Al
Loading (metal atoms/node)	4.5	3.3	2.8	3.4	4.2	7.3	4.5	3.3	4.7	5.0	4.2	4.3	7.0

https://dx.doi.org/10.1021/jacs.0c08641
J. Am. Chem. Soc. XXXX, XXX, XXX−XXX

thermal conductivity detector (TCD) and 2 flame ionization detectors (FID). The gas products identified were acetylene, ethylene, ethane, propadiene, propylene, and propane from the reactions as follows

$$\text{Isomerization: } C_3H_{4(g)}(\text{propyne}) \rightarrow C_3H_{4(g)}(\text{propadiene}) \quad \Delta H_r = 3.8 \pm 2.1 \text{ kJ/mol}$$

$$\text{Acetylene Formation: } C_3H_{4(g)}(\text{propyne}) + H_{2(g)} \rightarrow C_2H_{2(g)}(\text{acetylene}) + CH_{4(g)} \quad \Delta H_r = -33.6 \text{ kJ/mol}$$

$$\text{Complete Hydrogenation: } C_3H_{4(g)}(\text{propyne}) + 2H_{2(g)} \rightarrow C_3H_{8(g)}(\text{propane}) \quad \Delta H_r = -289.2 \text{ kJ/mol}$$

$$C_2H_{2(g)}(\text{acetylene}) + 2H_{2(g)} \rightarrow C_2H_{6(g)}(\text{ethane}) \quad \Delta H_r = -310.5 \text{ kJ/mol}$$

$$\text{PartialHydrogenation: } C_3H_{4(g)}(\text{propyne}) + H_{2(g)} \rightarrow C_3H_{6(g)}(\text{propene}) \quad \Delta H_r = -165 \text{ kJ/mol}$$

$$C_2H_{2(g)}(\text{acetylene}) + H_{2(g)} \rightarrow C_2H_{4(g)}(\text{ethene}) \quad \Delta H_r = -174.2 \text{ kJ/mol}$$

Initially, the catalysts were not pretreated; however, for the durability experiments, the catalysts were pretreated in 3.5% H_2 in Ar at 200 °C for 2 h.

PXRD of Metalated NU-1000 Samples. Powder X-ray diffraction (PXRD) patterns were taken on a Bruker Advance D8 Powder X-ray diffractometer with Ni-filtered Cu Kα radiation operating at 40 kV and 40 mA. The scan range was between 2° and 20° with 0.01° steps at a collection speed of 1 s/step.

ICP-OES of Metalated NU-1000 Samples. The number of metal atoms per Zr_6 node was confirmed using a ThermoFisher Scientific iCAP 7200 inductively coupled plasma-optical emission spectrometry (ICP-OES) system; ~1 mg of metalated NU-1000 was dissolved using 1 mL Piranha solution (3:1 99.999% sulfuric acid to 30 wt % hydrogen peroxide solution) in a 25 mL volumetric flask followed by a gentle sonication. **Caution**: since Piranha solution (H2SO4/30% H2O2, 7:3) reacts violently with many organic compounds, extreme care must be taken when handling it. Once metalated NU-1000 was fully dissolved, 24 mL of RO water was added for ICP-OES measurements.

Thermogravimetric Analysis (TGA) of Metalated NU-1000 samples. TGA of around 5 mg of sample was performed using a Discovery (TA Instruments) under a flow of N_2 of 10 mL/min at a heating rate of 5 °C/min from room temperature to 300 °C, followed by 1 h at 300 °C.

Difference Envelope Density (DED) Analysis. X-ray powder diffraction data were collected at beamline 11-ID-B of the Advanced Photon Source at Argonne National Laboratory using high energy X-rays (λ = 0.2114 Å). The detector geometry was calibrated and X-ray scattering images were reduced to one-dimensional diffraction data within GSAS-II.[28] The peak intensities in the diffraction data were quantified via Le Bail whole-pattern fitting[29] based on the reported structural model for NU-1000 (csq topology, *P*6/*mmm*, a ~ 40 Å, c ~ 17 Å). Structure envelopes were generated using the intensities of low-index reflections.[30,31] DEDs were then obtained via subtraction of the envelope for pristine NU-1000 from the envelope for ALD modified NU-1000 as described previously.[32,33]

Computational Details. Geometry optimizations and frequency calculations were performed using the M06-L local density functional[34] and an automatic density fitting on the ultrafine grid in Gaussian 09 software package.[35] The Def2-SVP basis was used for the C, H, O atoms and Def2-TZVP basis for the transition metals (Cu, Zn, Zr).[36] The SDD pseudopotential was used for the Zr atoms in the node.[37] Vibrational frequency calculations were performed for each optimized structure to verify the nature of each stationary point and to calculate thermochemical quantities at 300 °C after setting up all frequencies below 50 cm^{-1} to 50 cm^{-1} when calculating the vibrational partition function. All thermodynamic quantities were calculated at 1.0 atm pressure and 1 M concentrations for all reactants. We performed single point calculations using two hybrid functionals, M06[38] and B3LYP[39], for select reaction pathways. Dispersion corrections using the D3(BJ)[40] method were added to the B3LYP but not to the M06 and M06-L functionals, as these have long-range dispersion terms built-in the functional.[38,41] Figures S24–S26 show that the relative electronic energies for M06-L, M06 and B3LYP-D3(BJ) show similar trends.

A cluster model (Figure S1) was obtained by extracting one node, $[Zr_6(\mu_3\text{-}O)_4(\mu_3\text{–}OH)_4(OH)_4(OH_2)_4]^{8+}$, from a Zr-NU-1000 crystal structure optimized with periodic boundary conditions.[42] The node was capped with formate anions that replace the linkers, $[Zr_6(\mu_3\text{-}O)_4(\mu_3\text{–}OH)_4(OH)_4(OH_2)_4](HCOO)_{8,}$ and the positions of the carbon atoms of the linker were kept frozen to model the constraints by the MOF framework. The model of the catalyst was obtained by adding the metal (+2) cation on one face of the node, $[M\ Zr_6(\mu_3\text{-}O)_5(\mu_3\text{–}OH)_3(OH)_5(OH_2)_3](HCOO)_8$. The water molecule and the μ-hydroxy groups on the face of the cluster with the metal atom were deprotonated to maintain neutrality of the cluster. This deprotonation is part of the ALD mechanism of the synthesis of the catalyst, based on previous work,[19] and does not affect the free energies of the catalytic reactions. The other three faces of the node were dehydrated by removing 3 water molecules, and 3 terminal hydroxyls, and 3 μ-oxo protons, $[M\ Zr_6(\mu_3\text{-}O)_8(OH)_2](HCOO)_8$.

The doublet and singlet spin states were considered for $Cu^{2+}(d^9)$ and $Zn^{2+}(d^{10})$, respectively. The optimized structures, single point energies, and thermodynamic quantities for each structure are reported in the SI.

■ RESULTS AND DISCUSSION

An initial survey of ALD-prepared metal-modified MOFs determined the most viable catalysts for selective propyne conversion to propadiene and propylene. NU-1000 was exposed to the appropriate ALD precursor to append Cu, Cd, Co, Fe, Ga, Mo, Ni, Sn, W, Mn, Zn, In, and Al to the zirconium node. The synthesis, structure, and electronic structure of the resulting metal cluster for many AIMs has already been established in previous literature, including Al,[21] Co,[20] Cu,[24] In,[26] Ni,[19] and Zn.[25,33] Techniques such as difference envelope density (DED) analyses have elucidated the location of metal clusters such as Co, whereas pair distribution function (PDF) analyses have evaluated changes to the local metal cluster environment, such as MOF node distortions. Scanning electron microscopy (SEM), energy-dispersive X-ray spectroscopy (EDX), transmission electron microscopy (TEM), and X-ray photoelectron spectroscopy (XPS) were also conducted on these catalysts to provide full structural detail after ALD modification. Previously unpublished DED analysis of the In, Ni, and Mn AIMs are also provided in the SI. These combined results show metal cluster formation primarily in the ~8 Å channels and little to no node distortion. All the catalysts previously studied included multiple metal atoms per zirconium node (ranging from 2–8), and only the most reactive of ALD precursors (e.g., $AlMe_3$) resulted in a degradation of crystallinity in the MOF. Precursors were chosen for the catalysts herein such that no degradation in crystallinity was observed within one ALD cycle.

Two sequential cycles of Mn (Mn–Mn), Zn (Zn–Zn), Co (Co–Co) or sequential cycles of Co and Zn (Co–Zn and Zn–Co) were also implemented to afford additional local metal environments. The sequencing of metal deposition appears to have a small effect on the loading of heterobimetallic AIMs. For example, Co–Zn contained 1.65 Co/Zr_6 node and 3.82

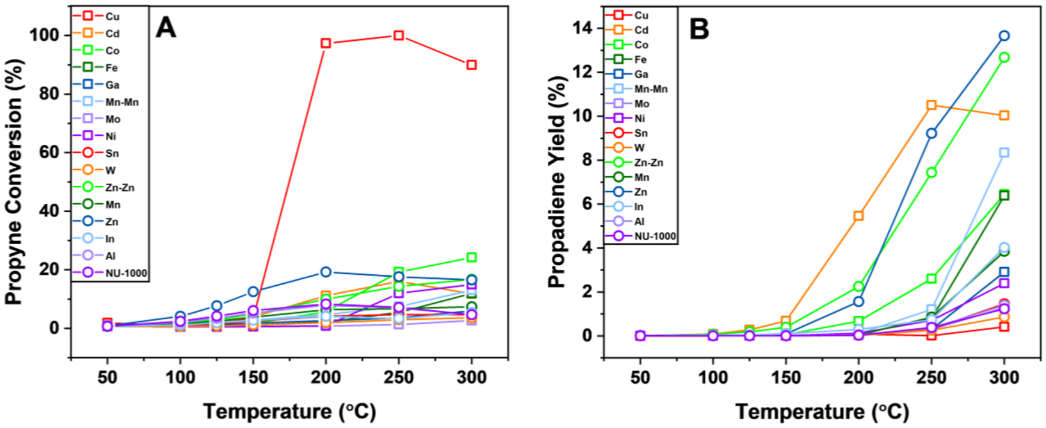

Figure 2. Propyne conversion (A) and propadiene yield (B) for various AIMs as a function of reaction temperature.

Zn/Zr_6 node, whereas Zn−Co contained 0.57 Co/Zr_6 node and 3.58 Zn/Zr_6 node. This is likely due to minute differences in the viable −OH sites of Zn clusters compared to Co clusters during nucleation. The highest selectivity to propadiene, given a 9.4 mL/min flow rate and 9.1 wt % catalyst loading at 300 °C, was found within Cd- and Zn-modified NU-1000 after a run time of ∼39 and ∼43 h, respectively. Maximum propadiene yields just prior to the end of the temperature sweep at 250 °C came from Cd-, Zn-, as well as Co-loaded MOFs (Figure 2). These metals were found to rise significantly beyond the diene yield of bare NU-1000, which is likely giving a small background isomerization due to either Zr interaction or thermodynamic equilibrium. Increasing the reaction temperature to 300 °C showed further increases in propadiene yield for Co, Fe, Zn, and In. It should be noted, however, that the Co-AIM selectivity to propadiene at 300 °C is comparable to that of the unmodified NU-1000 (Figure S2). A small drop in conversion for Cd from 250 to 300 °C coincides with an increase (albeit small) in acetylene production, which may indicate either a degradation in the MOF structure or cluster sintering when heating up to 300 °C.

While many of the metals tested catalyze the isomerization of propyne to propadiene, Cd and Zn were found to be the most effective. The efficacy of Cd- and Zn-modified NU-1000 for isomerization compared to the other catalysts may be due to the basic character of the metal oxide sites and their ability to instigate a 1,3-hydrogen shift for alkynes,[43] assuming the mechanism is similar across most AIMs. Previous isomerization literature has shown basic metal oxides to abstract and shuttle the methyl H to the terminal alkyne in accordance with their basicity.[8,44] Calculations discussed later point to this mechanism in the Zn-AIM. It should be noted that isomerization occurs in the absence of hydrogen as well. Preliminary experiments with Co, Cu, Cd, In, and Zn AIMs without H_2 and at low propyne conversions (<20%) show up to 100% selectivity to the isomer from 50 to 250 °C, as there are few competing mechanisms other than oligomerization. Obviously, these conditions yield no hydrogenation products.

Selective partial hydrogenation to propylene was also observed to varying extents (Figures S3−S4). The Cu-modified NU-1000 overwhelmingly produced more propylene than any other AIM (98.3% yield, 98.3% selectivity). This is unsurprising, however, as Cu has been well-known to catalyze the selective hydrogenation of propyne to propylene.[45] The Cu-AIM, however, compares favorably in yield and selectivity to other Cu catalysts (e.g., $Cu@SiO_2$) from the literature.[45,46] The only active metal catalysts for propylene above 250 °C were Zn, Co, and Ni. Propylene selectivity decreased upon metalation for almost all other AIM catalysts compared to bare NU-1000. It should be noted that conversion of propyne for all metal catalysts under these conditions either remained around the same level as NU-1000 or rose above the bare MOF when T ≥ 200 °C.

Full hydrogenation to propane was most prevalent in Zn-containing NU-1000 (Figures S5−S6), although the Zn-AIM exhibits the highest propyne conversion at lower temperatures when compared to other catalysts. At 150 °C, for example, Zn-AIM exhibited 12.5% propyne conversion compared to the 6.1% conversion for NU-1000. A decrease in propane yield from single exposures of metal precursors to double exposures results in a drop in propane yield (see Zn−Zn- and Mn−Mn-modified NU-1000 in Figure S5), even though propyne conversions did not change significantly. It is possible an increase in metal sites decreases the propensity for full hydrogenation while increasing the propensity for another reaction, such as partial hydrogenation or isomerization. An increase in the isomerization reaction can be seen in Mn−Mn, whereas Zn−Zn results in a small increase in partial hydrogenation when compared their single-dose counterparts.

To understand the difference in selectivity between different metal ions, computations were performed on the two extreme cases, namely, Zn^{2+} and Cu^{2+} deposited catalysts, that show the highest and the lowest selectivity, respectively, for isomerization among the first-row transition metals at 300 °C. These metals were also chosen as comparative models for hydrogenation due to their difference in performance. A single metal atom model was used despite characterization showing multiple metal atoms due to the preference metal ions have to occupy different faces of the Zr node in computational models, as highlighted in Li et al.[19]

First, the mechanism for hydrogenation would involve the splitting of the H_2 being flown over the catalyst. Different metal ions could promote either homolytic or heterolytic splitting of H_2 (Figure 3) and thus might have different mechanisms for the reaction. Table 2 shows the computed reaction enthalpies and free energies per H_2 molecule for the two different reactions.

While in the heterolytic splitting reaction 1 the oxidation state of the metal does not change, in reaction 2, the addition of a hydrogen atom arising from the homolytic splitting leads to a reduction of the metal from a +II oxidation state to +I as the electron is accepted by the metal ion and the proton bonds

https://dx.doi.org/10.1021/jacs.0c08641
J. Am. Chem. Soc. XXXX, XXX, XXX−XXX

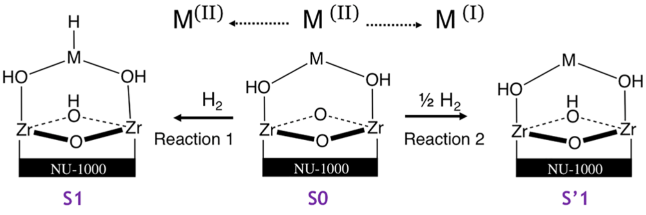

Figure 3. Reaction scheme for two possible hydrogen splitting pathways as reaction 1 and reaction 2.

Table 2. Reaction Enthalpies and Gibbs Free Energies (in Parentheses) Per Hydrogen Molecule (kcal/mol) for Dissociation over Cu and Zn as Calculated Per the Scheme Shown in Figure 3

Metal	Reaction 1	Reaction 2
Cu	−15.9 (1.6)	−72.4 (−51.2)
Zn	−20.1 (−5.2)	24.3 (34.6)

to the μ-oxo. Whereas Cu prefers the +I oxidation state with the d^{10} electron configuration, Zn has the stable d^{10} configuration in the + II oxidation state. This is reflected in the reaction energies in Table 2. This suggests the resting state of the Cu catalysts will more likely have the copper in the more stable +1 oxidation state under H_2. In contrast, for Zn^{2+}, heterolytic H_2 splitting is energetically much more favorable. Throughout the reaction pathways for Zn, the overall spin state remains a singlet while for the Cu, the doublet and singlet spin states are considered, respectively, for intermediates with formal Cu^{2+} and Cu^{1+} oxidation states.

Thermogravimetric analysis (TGA) of the catalysts suggested presence of water in the system for the Zn catalyst around this temperature (Figures S7−S11). The model thus includes one water molecule bound to Zn that is involved in the mechanism for isomerization. However, the water molecule does not bind to the zinc hydride and is thus not included in hydrogenation. Optimized structures of clusters with water bound to the bare metal and to the metal hydride, albeit weakly, are shown in Figure S12 Neither the hydrogenation nor isomerization mechanism proposed for Cu involves this water molecule as the TGA of the Cu catalyst showed the last peak at around 230 °C, which is approximately when the catalyst starts to exhibit the higher selectivity toward hydrogenation.

Previous proposed mechanisms for hydrogenation of unsaturated hydrocarbons on AIM catalysts deposited in NU-1000 were based on a heterolytic splitting of H_2 with the formation of a metal hydride (H1) as shown in Scheme 1.[19] This is obtained by heterolytic splitting of a hydrogen molecule over the dehydrated catalyst structure shown in Figure 3.

The adsorption of propyne is followed by the transfer of the hydride to the terminal carbon forming a metal−carbon bond ($H3_{A/B}$). The hydride can then either transfer to the β-carbon and the metal can form a bond with the terminal carbon (path A) or the other way around (path B). Another hydrogen molecule then adsorbs on the metal ($H4_{A/B}$) and splits heterolytically forming back the metal hydride, while the proton attacks the β-carbon to form propene (H5). The relative Gibbs free energies for this hydrogenation mechanism for both Cu and Zn are reported in Table 3. The Gibbs free energy barrier for Cu (path A) is 36.6 kcal/mol, and that for Zn (pathway B) is 53.3 kcal/mol (see Figure S13). A possible rationale for TS23 in pathways A and B having different relative energies is the extent to which the C−C−C bond angle in propyne deviates from the 180° starting point. As seen in Figure S27, the $TS23_A$ undergoes smaller distortion in Cu while for the Zn catalyst, the $TS23_B$ has a smaller bending of the angle compared to that of their other counterpart.

Table 3. Relative Gibbs Free Energies (kcal/mol) Calculated at 300 °C for Both Hydrogenation Pathways Shown in Figure 5 for Cu and Zn

	H1	H2	TS-$23_{A/B}$	$H3_{A/B}$	$H4_{A/B}$	TS-$45_{A/B}$	H5
Cu (path A)	0.0	9.1	18.7	−17.8	−7.8	14.1	−11.9
Cu (path B)	0.0	9.1	23.2	−17.2	−7.2	13.5	−11.9
Zn (path A)	0.0	12.3	41.1	−12.3	−3.0	32.5	−13.3
Zn (path B)	0.0	12.3	38.0	−15.3	−3.0	30.4	−13.3

In the hydrogenation mechanism proposed in Scheme 1, the formal oxidation state of the metal does not change as the hydrogen splits heterolytically. The hydrogenation mechanism involving homolytic splitting of H_2 through which the reaction may undergo for Cu is shown in Scheme 2.

Scheme 1. Reaction Mechanism for Hydrogenation Involving the Heterolytic Splitting of Dihydrogen

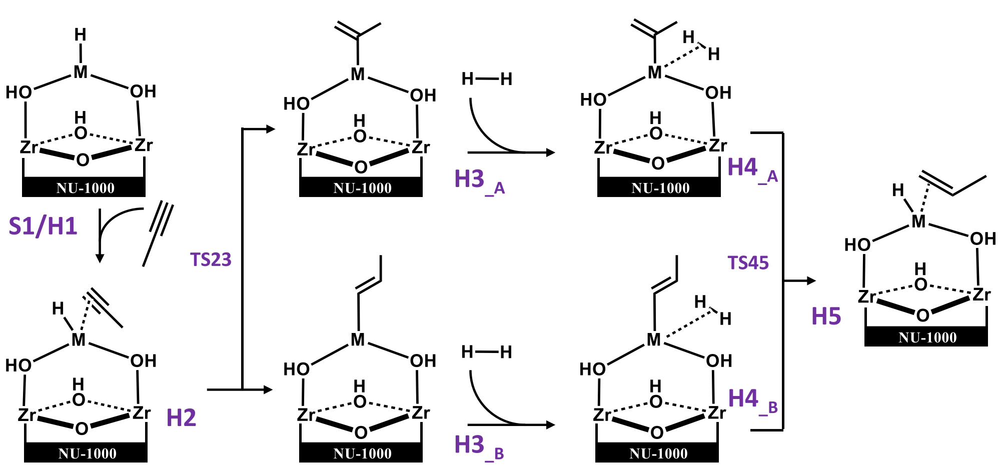

Scheme 2. Reaction Mechanism for Hydrogenation Involving the Homolytic Splitting of Dihydrogen[a]

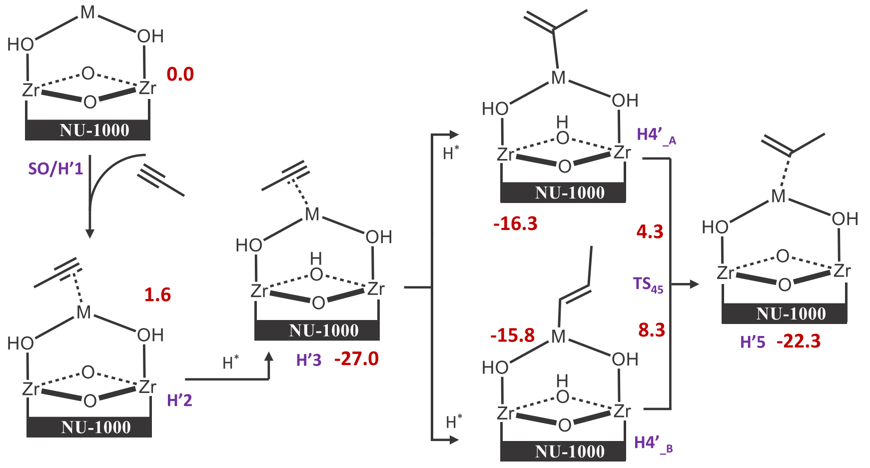

[a]The relative free energies in kcal/mol calculated for reactions over Cu are noted along with the intermediates.

Scheme 3. Isomerization Mechanisms Involving Zn^{2+} (Left) and Cu^{1+} (Right) along with Their Respective Relative Free Energies (kcal/mol) Calculated at 300 °C

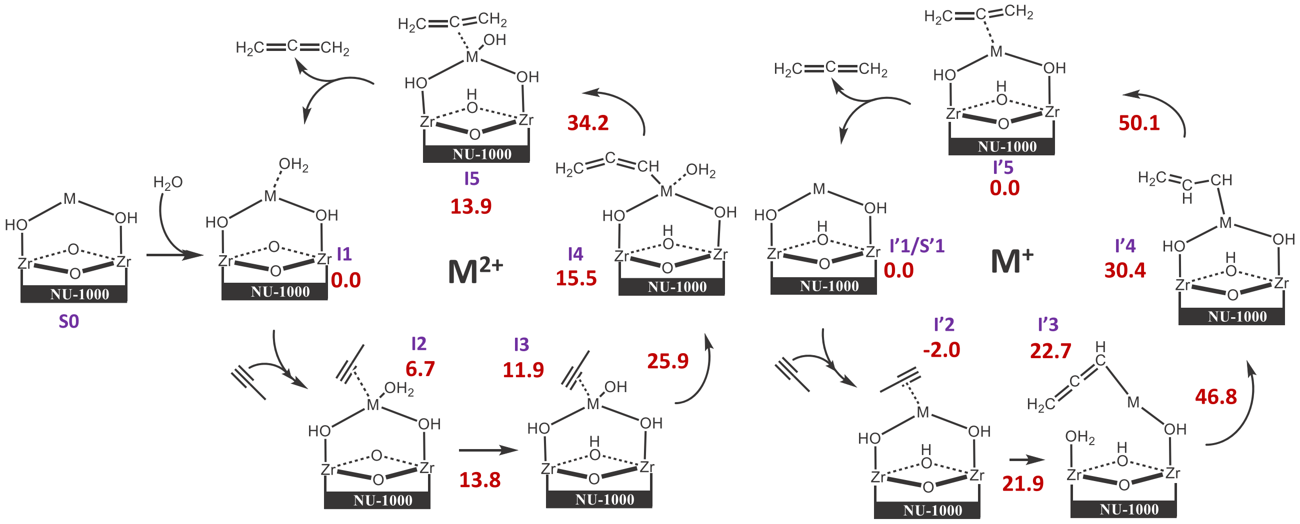

The first addition of the hydrogen atom to H’2 leads to the reduction of copper (H’3) as it accepts the incoming electron while the proton bonds to the μ-oxo. The subsequent addition of the other hydrogen atom on the adsorbed propyne results in the formation of a metal−carbon bond. This changes the formal oxidation state of the metal to +II in the intermediate $H'4_{A/B}$. Like in Scheme 1, both possibilities of the metal−carbon in $H'4_{A/B}$ were studied as paths A and B. The hydrogenation process is then completed as the proton of the μ-hydroxy is abstracted (TS-45) to form propene. The relative free energies for both the pathways are noted alongside each intermediate in Scheme 2. The Gibbs free energy barrier is 31.3 kcal/mol for the hydrogenation showing that this pathway is preferred over the one involving heterolytic splitting of H_2.

The isomerization mechanism for Zn in Scheme 3 involve a heterolytic splitting of a water molecule over Zn forming a metal-hydroxy bond. The hydroxy group then acts as a shuttle for the proton between the methyl group and the terminal carbon for the 1,3-hydrogen shift. The Gibbs free energy barrier for Zn in this mechanism was found to be 34.2 kcal/mol. When compared to the free energy of activation for hydrogenation, which is 53.3 kcal/mol, this explains the selectivity of Zn toward the isomerization product. This mechanism was also studied for Cu^{2+} (see SI for details). But as previously established, the Cu catalyst will have the Cu in a + I oxidation state and thus a mechanism involving Cu^{+} must be considered here.

This mechanism for isomerization does not cycle through the + I/+II oxidation state of the Cu. This is along similar lines as the mechanism reported for Zn. But since there is no heterolytic splitting of water over the metal ion, the mechanism goes through opening of the metal ion− terminal hydroxy bond. This hydroxy group then acts as the shuttle for the proton. Unlike the previous isomerization mechanism however, this migration is stepwise. The hydroxy shuttles the proton only between the α and the β carbons. The product is formed after a 2,3-hydrogen shift which is the rate determining step of the reaction. The reaction energies reported in Scheme 3 show the free energy of activation to be 52.1 kcal/mol for the isomerization over a Cu^{+} species.

To identify synergistic effects between multiple proximal catalytic metal sites, as well as determine the effect of reaction conditions, variable pressure and time studies were conducted on Co and Zn bimetallic combinations. In the pressure studies,

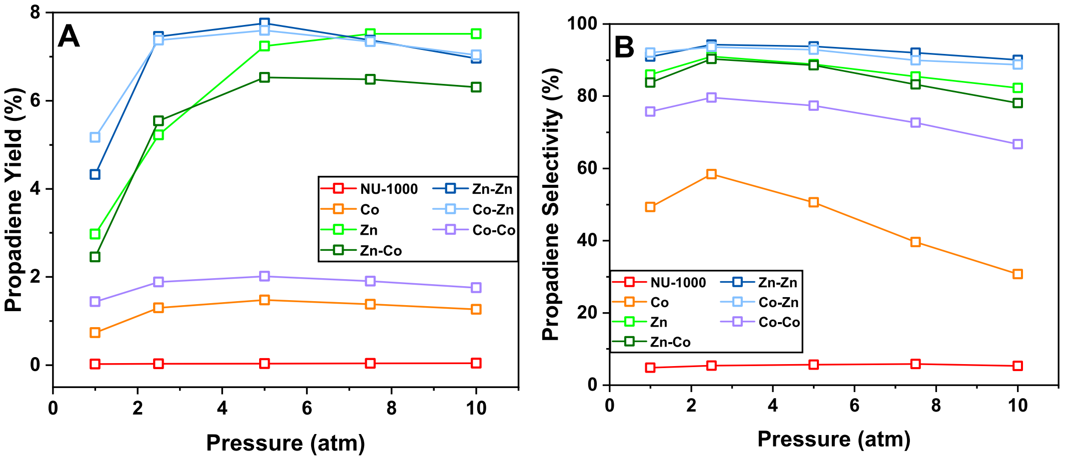

Figure 4. Propadiene yield (A) and selectivity (B) for Co- and Zn-modified MOFs as a function of reaction pressure.

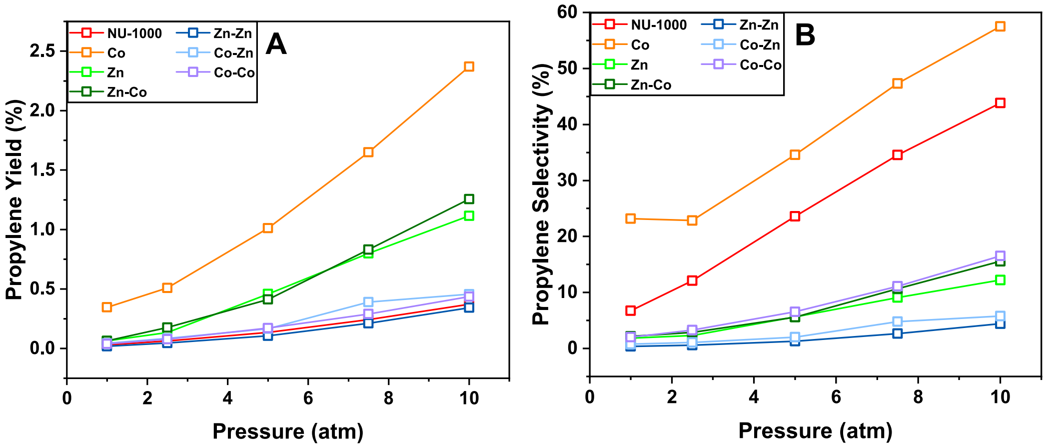

Figure 5. Propylene yield (A) and selectivity (B) for Co- and Zn-modified MOFs as a function of reaction vessel pressure.

the incorporation of Co into Zn-modified NU-1000 showed high yields and selectivity toward propadiene compared to monometallic Co-modified NU-1000. The Co−Zn and Zn−Co MOFs also exhibited low propylene yields and selectivity compared to the standalone Co-AIM (Figures 4 and 5). These bimetallic modified MOFs also exhibited lower propane yields, compared to those of the standalone Zn-AIM (Figure S6), as well as decreased either the extent of coking or the production of other unidentified products compared to the Co-AIM (see carbon balance in SI). These results suggest a synergistic effect for the isomerization of propyne by Co- and Zn-modified NU-1000 where the creation of side products (propylene, propane, coke) is mitigated through bimetallic sites that inhibit the hydrogenation and coking pathways. Increasing the reaction pressure beyond 5 atm does, however, result in a slight decrease in propadiene yield and selectivity while increasing the yield and selectivity of propylene and propane. It is possible that an abundance of hydrogen shifts the equilibrium away from isomerization and toward hydrogenation if the metal oxide cannot effectively shuttle H from the methyl group to the terminal alkyne. Additionally, this does not appear to influence the extent of coking via changes in reaction pressure, if there is any coking at all. This may be due to the coking mechanism being dependent on the formation of radicals.[47] The difference in propadiene yield between Zn−Co- and Co−Zn-modified NU-1000 may be due to which metal atoms occupy the exterior of the cluster, as the amount of Co and Zn atoms is approximately the same for both MOFs (Figure S14 for ICP data). The AIM with secondary exposure to Zn (i.e., Co−Zn MOF) has a higher propadiene yield and selectivity, which coincides with the high propadiene activity of the standalone Zn-modified MOF.

Co- and Zn-MOFs were also monitored for ∼24 h at various temperatures to evaluate deactivation and overall changes in catalytic behavior (Figures S15, S16). For conversion to propadiene, many of the Co-containing MOFs (i.e., Co−Co at 250 °C and Co at 300 °C) showed an increase in activity and selectivity as the reaction progressed toward 24 h, indicative of an induction period. The induction period is likely due to the reduction of Co by the hydrogen feed gas at the beginning of the reaction. By contrast, a slight deactivation can be seen well after 16 h in some Zn-containing MOFs, most noticeably with Zn−Co at 250 °C and Zn−Zn at 250 °C catalysts. The deactivation does not appear to be due to blocking of the active Zn sites by coke, however, as the carbon balance stays relatively the same and high throughout the experiment (Figures S17−S19). Zn and Co−Zn MOFs at 300 °C required little to no induction period nor deactivation while providing sizable yields and high selectivity, and thus appear to be the most effective catalysts for propyne isomerization to propadiene.

Powder XRD of the Zn and Co bimetallic combinations show the crystalline structure of NU-1000 remains intact for Zn−Co, Co−Zn, and Zn−Zn samples, while Co−Co appears

https://dx.doi.org/10.1021/jacs.0c08641
J. Am. Chem. Soc. XXXX, XXX, XXX−XXX

to lose its ordered crystalline structure after deposition (Figure S20). The ICP-derived loading of Co−Co is consistent with degradation of the MOF framework, as the number of Co metal atoms per Zr_6 node (>20 atoms) was measured to be much larger than what is controllably achieved (Figure S14). Other AIM-modified MOFs exhibited <7 metal atoms on each node, as previously observed for well-controlled reactions with NU-1000 nodes. It is possible that a collapse in MOF structure occurs during the second exposure of NU-1000 to the Co precursor. This change in structure may also be responsible for the significant decrease in propyne conversion between single and double exposure Co AIMs (Figure S21). It is unclear as to why double Co precursor exposures causes a degradation in structure, although follow-up experiments are planned.

■ CONCLUSIONS

The survey of metalations for MOFs conducted herein show multiple avenues for biasing a reaction system toward a certain product while also allowing for a reduction in undesirable products through synergistic effects. Certain metals, such as Zn, Cd, and In, exhibited a high selectivity toward the propyne isomer under H_2 while showing a smaller affinity toward partial hydrogenation and no oligomerization. Other metals, such as Cu and Co, showed a larger affinity toward partial hydrogenation. While full hydrogenation was limited for all metals, further reductions in propane production were found with particular metal combinations. For example, a combination of Co with Zn resulted in a reduction of propane across all experimental parameters surveyed when compared to the standalone metals with as much as a 78% reduction in propane yield. The incorporation of Zn into Co-AIMs also reduced coking and oligomerization: undesirable side reactions that can reduce the efficacy of alkyne and alkene transformation catalysts. The preference for isomerization vs partial hydrogenation in the case of Zn and Cu lies in their respective preferences for heterolytic vs homolytic H_2 cleavage and H shuttling mechanism between 1,3- or 2,3-hydrogen shift, with the latter being more costly energetically. Isomerization was found to be more energetically favorable than partial hydrogenation in Zn-AIM by 19.1 kcal/mol, whereas partial hydrogenation was more favorable in Cu-AIM when compared to isomerization by 20.8 kcal/mol. These results highlight the potential for high-throughput testing and extensive metal surveying when looking at solutions for extensive reaction systems.

■ ASSOCIATED CONTENT

Supporting Information

The Supporting Information is available free of charge at https://pubs.acs.org/doi/10.1021/jacs.0c08641.

Synthesis and characterization of Zn-AIM, Co-AIM, Cd-AIM, Cu-AIM, Fe-AIM, Ga-AIM, Mn-AIM, Mo-AIM, Ni-AIM, Sn-AIM, W-AIM, In-AIM, and Al-AIM (PDF)

■ AUTHOR INFORMATION

Corresponding Authors

Joachim Sauer − *Institut für Chemie, Humboldt-Universität zu Berlin, 10099 Berlin, Germany;* orcid.org/0000-0001-6798-6212; Email: js@chemie.hu-berlin.de

Laura Gagliardi − *Department of Chemistry, Chemical Theory Center, and Supercomputing Institute, University of Minnesota-Twin Cities, Minneapolis, Minnesota 55455, United States;* orcid.org/0000-0001-5227-1396; Email: gagliard@umn.edu

Alex B. F. Martinson − *Materials Science Division, Argonne National Laboratory, Lemont, Illinois 60439, United States;* orcid.org/0000-0003-3916-1672; Email: martinson@anl.gov

Massimiliano Delferro − *Chemical Sciences and Engineering Division, Argonne National Laboratory, Lemont, Illinois 60439, United States;* orcid.org/0000-0002-4443-165X; Email: delferro@anl.gov

Authors

Ryan A. Hackler − *Chemical Sciences and Engineering Division, Argonne National Laboratory, Lemont, Illinois 60439, United States;* orcid.org/0000-0003-4698-6074

Riddhish Pandharkar − *Department of Chemistry, Chemical Theory Center, and Supercomputing Institute, University of Minnesota-Twin Cities, Minneapolis, Minnesota 55455, United States*

Magali S. Ferrandon − *Chemical Sciences and Engineering Division, Argonne National Laboratory, Lemont, Illinois 60439, United States*

In Soo Kim − *Materials Science Division, Argonne National Laboratory, Lemont, Illinois 60439, United States; Nanophotonics Research Center, Korea Institute of Science and Technology (KIST), Seoul 02792, Republic of Korea*

Nicolaas A. Vermeulen − *Department of Chemistry, Northwestern University, Evanston, Illinois 60208, United States*

Leighanne C. Gallington − *X-ray Science Division, Argonne National Laboratory, Lemont, Illinois 60439, United States;* orcid.org/0000-0002-0383-7522

Karena W. Chapman − *Department of Chemistry, Stony Brook University, Stony Brook, New York 11764, United States;* orcid.org/0000-0002-8725-5633

Omar K. Farha − *Department of Chemistry, Northwestern University, Evanston, Illinois 60208, United States;* orcid.org/0000-0002-9904-9845

Christopher J. Cramer − *Department of Chemistry, Chemical Theory Center, and Supercomputing Institute, University of Minnesota-Twin Cities, Minneapolis, Minnesota 55455, United States;* orcid.org/0000-0001-5048-1859

Complete contact information is available at: https://pubs.acs.org/10.1021/jacs.0c08641

Author Contributions

[$] These authors contributed equally

Notes

The authors declare no competing financial interest.

■ ACKNOWLEDGMENTS

This work was supported as part of the Inorganometallic Catalyst Design Center, an Energy Frontier Research Center funded by the U.S. Department of Energy, Office of Science, Basic Energy Sciences under Award No. DE-SC0012702. J.S. acknowledges support by Deutsche Forschungsgemeinschaft (DFG, German Research Foundation) within project 430942176. This work also used the Advanced Photon Source, a U.S. Department of Energy (DOE) Office of Science User Facility operated for the DOE Office of Science by Argonne National Laboratory under Contract No. DE-AC02-06CH11357.

■ REFERENCES

(1) Burch, R.; Hayes, M. J. C-H bond activation in hydrocarbon oxidation on solid catalysts. *J. Mol. Catal. A: Chem.* **1995**, *100* (1−3), 13−33.

(2) Zaera, F. Surface chemistry of hydrocarbon fragments on transition metals: towards understanding catalytic processes. *Catal. Lett.* **2003**, *91* (1−2), 1−10.

(3) Studt, F.; Abild-Pedersen, F.; Bligaard, T.; Sorensen, R. Z.; Christensen, C. H.; Norskov, J. K. Identification of non-precious metal alloy catalysts for selective hydrogenation of acetylene. *Science* **2008**, *320* (5881), 1320−1322.

(4) Tysoe, W. T.; Nyberg, G. L.; Lambert, R. M. Low-Temperature Catalytic Chemistry of the Pd(111) Surface - Benzene and Ethylene from Acetylene. *J. Chem. Soc., Chem. Commun.* **1983**, No. 11, 623−625.

(5) Molnar, A.; Sarkany, A.; Varga, M. Hydrogenation of carbon-carbon multiple bonds: chemo-, regio- and stereo-selectivity. *J. Mol. Catal. A: Chem.* **2001**, *173* (1−2), 185−221.

(6) Hoffmann-Roder, A.; Krause, N. Synthesis and properties of allenic natural products and pharmaceuticals. *Angew. Chem., Int. Ed.* **2004**, *43* (10), 1196−216.

(7) Zimmer, R.; Dinesh, C. U.; Nandanan, E.; Khan, F. A. Palladium-catalyzed reactions of allenes. *Chem. Rev.* **2000**, *100* (8), 3067−126.

(8) Hashmi, A. S. K., Synthesis of Allenes by Isomerization Reactions. In *Modern Allene Chemistry*, Krause, N.; Hashmi, A. S. K., Eds. Wiley-VCH Verlag GmbH & Co: 2004.

(9) Parmentier, J. H.; Peer, H. G.; Schutte, L. The Isomerization of Propyne into Propadiene Over a Silica Catalyst. *J. Catal.* **1971**, *22*, 213−218.

(10) Vermeulen, N. A.; Karagiaridi, O.; Sarjeant, A. A.; Stern, C. L.; Hupp, J. T.; Farha, O. K.; Stoddart, J. F. Aromatizing olefin metathesis by ligand isolation inside a metal-organic framework. *J. Am. Chem. Soc.* **2013**, *135* (40), 14916−14919.

(11) Syed, Z. H.; Sha, F.; Zhang, X.; Kaphan, D. M.; Delferro, M.; Farha, O. K. Metal-Organic Framework Nodes as a Supporting Platform for Tailoring the Activity of Metal Catalysts. *ACS Catal.* **2020**, *10*, 11556.

(12) Cui, Y. J.; Li, B.; He, H. J.; Zhou, W.; Chen, B. L.; Qian, G. D. Metal-Organic Frameworks as Platforms for Functional Materials. *Acc. Chem. Res.* **2016**, *49* (3), 483−493.

(13) Lee, J.; Farha, O. K.; Roberts, J.; Scheidt, K. A.; Nguyen, S. T.; Hupp, J. T. Metal-organic framework materials as catalysts. *Chem. Soc. Rev.* **2009**, *38* (5), 1450−1459.

(14) Liu, L.; Corma, A. Metal Catalysts for Heterogeneous Catalysis: From Single Atoms to Nanoclusters and Nanoparticles. *Chem. Rev.* **2018**, *118* (10), 4981−5079.

(15) Deria, P.; Mondloch, J. E.; Tylianakis, E.; Ghosh, P.; Bury, W.; Snurr, R. Q.; Hupp, J. T.; Farha, O. K. Perfluoroalkane Functionalization of NU-1000 via Solvent-Assisted Ligand Incorporation: Synthesis and CO$_2$ Adsoprtion Studies. *J. Am. Chem. Soc.* **2013**, *135*, 16801−16804.

(16) Mondloch, J. E.; Bury, W.; Fairen-Jimenez, D.; Kwon, S.; DeMarco, E. J.; Weston, M. H.; Sarjeant, A. A.; Nguyen, S. T.; Stair, P. C.; Snurr, R. Q.; Farha, O. K.; Hupp, J. T. Vapor-phase metalation by atomic layer deposition in a metal-organic framework. *J. Am. Chem. Soc.* **2013**, *135* (28), 10294−10297.

(17) George, S. M. Atomic layer deposition: an overview. *Chem. Rev.* **2010**, *110* (1), 111−31.

(18) Kim, I. S.; Li, Z.; Zheng, J.; Platero-Prats, A. E.; Mavrandonakis, A.; Pellizzeri, S.; Ferrandon, M.; Vjunov, A.; Gallington, L. C.; Webber, T. E.; Vermeulen, N. A.; Penn, R. L.; Getman, R. B.; Cramer, C. J.; Chapman, K. W.; Camaioni, D. M.; Fulton, J. L.; Lercher, J. A.; Farha, O. K.; Hupp, J. T.; Martinson, A. B. F. Sinter-Resistant Platinum Catalyst Supported by Metal-Organic Framework. *Angew. Chem., Int. Ed.* **2018**, *57* (4), 909−913.

(19) Li, Z.; Schweitzer, N. M.; League, A. B.; Bernales, V.; Peters, A. W.; Getsoian, A. B.; Wang, T. C.; Miller, J. T.; Vjunov, A.; Fulton, J. L.; Lercher, J. A.; Cramer, C. J.; Gagliardi, L.; Hupp, J. T.; Farha, O. K. Sintering-Resistant Single-Site Nickel Catalyst Supported by Metal-Organic Framework. *J. Am. Chem. Soc.* **2016**, *138* (6), 1977−82.

(20) Li, Z. Y.; Peters, A. W.; Bernales, V.; Ortuno, M. A.; Schweitzer, N. M.; DeStefano, M. R.; Gallington, L. C.; Platero-Prats, A. E.; Chapman, K. W.; Cramer, C. J.; Gagliardi, L.; Hupp, J. T.; Farha, O. K. Metal-Organic Framework Supported Cobalt Catalysts for the Oxidative Dehydrogenation of Propane at Low Temperature. *ACS Cent. Sci.* **2017**, *3* (1), 31−38.

(21) Rimoldi, M.; Bernales, V.; Borycz, J.; Vjunov, A.; Gallington, L. C.; Platero-Prats, A. E.; Kim, I. S.; Fulton, J. L.; Martinson, A. B. F.; Lercher, J. A.; Chapman, K. W.; Cramer, C. J.; Gagliardi, L.; Hupp, J. T.; Farha, O. K. Atomic Layer Deposition in a Metal-Organic Framework: Synthesis, Characterization, and Performance of a Solid Acid. *Chem. Mater.* **2017**, *29* (3), 1058−1068.

(22) Peters, A. W.; Li, Z.; Farha, O. K.; Hupp, J. T. Atomically Precise Growth of Catalytically Active Cobalt Sulfide on Flat Surfaces and within a Metal-Organic Framework via Atomic Layer Deposition. *ACS Nano* **2015**, *9*, 8484−8490.

(23) Zhang, X.; Huang, Z.; Ferrandon, M.; Yang, D.; Robison, L.; Li, P.; Wang, T. C.; Delferro, M.; Farha, O. K. Catalytic Chemoselective Functionalization of Methane in a Metal-Organic Framework. *Nat. Catal.* **2018**, *1*, 356−362.

(24) Platero-Prats, A. E.; Li, Z.; Gallington, L. C.; Peters, A. W.; Hupp, J. T.; Farha, O. K.; Chapman, K. W. Addressing the characterisation challenge to understand catalysis in MOFs: the case of nanoscale Cu supported in NU-1000. *Faraday Discuss.* **2017**, *201*, 337−350.

(25) Kim, I. S.; Ahn, S.; Vermeulen, N. A.; Webber, T. E.; Gallington, L. C.; Chapman, K. W.; Penn, R. L.; Hupp, J. T.; Farha, O. K.; Notestein, J. M.; Martinson, A. B. F. The Synthesis Science of Targeted Vapor-Phase Metal-Organic Framework Postmodification. *J. Am. Chem. Soc.* **2020**, *142* (1), 242−250.

(26) Kim, I. S.; Borycz, J.; Platero-Prats, A. E.; Tussupbayev, S.; Wang, T. C.; Farha, O. K.; Hupp, J. T.; Gagliardi, L.; Chapman, K. W.; Cramer, C. J.; Martinson, A. B. F. Targeted Single-Site MOF Node Modification: Trivalent Metal Loading via Atomic Layer Deposition. *Chem. Mater.* **2015**, *27* (13), 4772−4778.

(27) Lownsbury, J. M.; Gladden, J. A.; Campbell, C. T.; Kim, I. S.; Martinson, A. B. F. Direct Measurements of Half-Cycle Reaction Heats during Atomic Layer Deposition by Calorimetry. *Chem. Mater.* **2017**, *29* (20), 8566−8577.

(28) Toby, B. H.; Von Dreele, R. B. GSAS-II: the genesis of a modern open-source all purpose crystallography software package. *J. Appl. Crystallogr.* **2013**, *46* (2), 544−549.

(29) Petříček, V.; Dušek, M.; Palatinus, L. Z. Crystallographic Computing System JANA2006: General features. *Z. Kristallogr. - Cryst. Mater.* **2014**, *229*, 345−352.

(30) Yakovenko, A. A.; Reibenspies, J. H.; Bhuvanesh, N.; Zhou, H.-C. Generation and applications of structure envelopes for porous metal-organic frameworks. *J. Appl. Crystallogr.* **2013**, *46* (2), 346−353.

(31) McCusker, L. B.; Baerlocher, C. Using electron microscopy to complement X-ray powder diffraction data to solve complex crystal structures. *Chem. Commun.* **2009**, 1439−1451.

(32) Yakovenko, A. A.; Wei, Z.; Wriedt, M.; Li, J.-R.; Halder, G. J.; Zhou, H.-C. Study of guest molecules in metal-organic frameworks by powder X-ray diffraction: analysis of difference envelope density. *Cryst. Growth Des.* **2014**, *14*, 5397−5407.

(33) Gallington, L. C.; Kim, I. S.; Liu, W. G.; Yakovenko, A. A.; Platero-Prats, A. E.; Li, Z.; Wang, T. C.; Hupp, J. T.; Farha, O. K.; Truhlar, D. G.; Martinson, A. B. F.; Chapman, K. W. Regioselective Atomic Layer Deposition in Metal-Organic Frameworks Directed by Dispersion Interactions. *J. Am. Chem. Soc.* **2016**, *138* (41), 13513−13516.

(34) Zhao, Y.; Truhlar, D. G. A new local density functional for main-group thermochemistry, transition metal bonding, thermochemical kinetics, and noncovalent interactions. *J. Chem. Phys.* **2006**, *125* (19), 194101.

(35) Frisch, M. J.; Trucks, G. W.; Schlegel, H. B.; Scuseria, G. E.; Robb, M. A.; Cheeseman, J. R.; Scalmani, G.; Barone, V.; Mennucci,

B.; Petersson, G. A.; Nakatsuji, H.; Caricato, M.; Li, X.; Hratchian, H. P.; Izmaylov, A. F.; Bloino, J.; Zheng, G.; Sonneberg, J. L.; Hada, M.; Ehara, M.; Toyota, K.; Fukuda, R.; Hasegawa, J.; Ishida, M.; Nakajima, T.; Honda, Y.; Kitao, O.; Nakai, H.; Vreven, T.; Montgomery, J. A.; Peralta, J. E.; Ogliaro, F.; Bearpark, M.; Heyd, J. J.; Brothers, E.; Kudin, K. N.; Staroverov, V. N.; Kobayashi, R.; Normand, J.; Raghavachari, K.; Rendell, A.; Burant, J. C.; Iyengar, S. S.; Tomasi, J.; Cossi, M.; Rega, N.; Millam, J. M.; Klene, M.; Knox, J. E.; Cross, J. B.; Bakken, V.; Adamo, C.; Jaramillo, J.; Gomperts, R.; Stratmann, R. E.; Yazyev, O.; Austin, A. J.; Cammi, R.; Pomelli, C.; Ochterski, J. W.; Martin, R. L.; Morokuma, K.; Zakrzewski, V. G.; Voth, G. A.; Salvador, P.; Dannenberg, J. J.; Dapprich, S.; Daniels, A. D.; Farkas, O.; Foresman, J. B.; Ortiz, J. V.; Cioslowski, J.; Fox, D. J. *Gaussian 09*, Revision B.01. Gaussian 09, Revision B.01, Gaussian, Inc., Wallingford CT, 2009.

(36) Weigend, F.; Ahlrichs, R. Balanced basis sets of split valence, triple zeta valence and quadruple zeta valence quality for H to Rn: Design and assessment of accuracy. *Phys. Chem. Chem. Phys.* **2005**, *7* (18), 3297−305.

(37) Andrae, D.; Häußermann, U.; Dolg, M.; Stoll, H.; Preuß, H. Energy-adjusted *ab initio* pseudopotentials for the second and third row transition elements. *Theoretica Chimica Acta* **1990**, *77*, 123−141.

(38) Zhao, Y.; Truhlar, D. G. The M06 suite of density functionals for main group thermochemistry, thermochemical kinetics, noncovalent interactions, excited states, and transition elements: two new functionals and systematic testing of four M06-class functionals and 12 other function. *Theor. Chem. Acc.* **2008**, *120* (1−3), 215−241.

(39) Becke, A. D. Density-functional thermochemistry. III. The role of exact exchange. *J. Chem. Phys.* **1993**, *98* (7), 5648−5652.

(40) Grimme, S.; Ehrlich, S.; Goerigk, L. Effect of the damping function in dispersion corrected density functional theory. *J. Comput. Chem.* **2011**, *32* (7), 1456−1465.

(41) Zhao, Y.; Truhlar, D. G. A new local density functional for main-group thermochemistry, transition metal bonding, thermochemical kinetics, and noncovalent interactions. *J. Chem. Phys.* **2006**, *125* (19), 194101−194101.

(42) Planas, N.; Mondloch, J. E.; Tussupbayev, S.; Borycz, J.; Gagliardi, L.; Hupp, J. T.; Farha, O. K.; Cramer, C. J. Defining the Proton Tpology of the Zr_6-Based Metal-Organic Framework NU-1000. *J. Phys. Chem. Lett.* **2014**, *5*, 3716−3723.

(43) Vitkovskaya, N. M.; Kobychev, V. B.; Trofimov, A. B.; Trofimov, B. A. Multiple bond migration with participation of a protophilic agent 1. An ab initio quantum-chemical study of 1,3-hydrogen shift in propene and propyne with participation of hydroxide ion. *Russ. Chem. Bull.* **1997**, *46*, 1677−1682.

(44) Hackler, L.; Konya, Z.; Kiricsi, I. Transformation of propyne to propadiene over various solid catalysts of different acid-base character. *React. Kinet. Catal. Lett.* **2001**, *74* (2), 363−370.

(45) Bridier, B.; Lopez, N.; Perez-Ramirez, J. Partial hydrogenation of propyne over copper-based catalysts and comparison with nickel-based analogues. *J. Catal.* **2010**, *269* (1), 80−92.

(46) Wehrli, J.T.; Thomas, D.J.; Wainwright, M.S.; Trimm, D.L.; Cant, N.W. Selective Hydrogenation of Propyne over an Ion-Exchanged Copper on Silica Catalyst. *Appl. Catal.* **1990**, *66* (1), 199−208.

(47) Wauters, S.; Marin, G. B. Kinetic Modeling of Coke Formation during Steam Cracking. *Ind. Eng. Chem. Res.* **2002**, *41*, 2379−2391.